JACS
JOURNAL OF THE AMERICAN CHEMICAL SOCIETY
Communication
Cite This: J. Am. Chem. Soc. 2017, 139, 16092-16095
pubs.acs.org/JACS

Ring-Fusion of Perylene Diimide Acceptor Enabling Efficient Nonfullerene Organic Solar Cells with a Small Voltage Loss

Jianquan Zhang,[†,‡] Yunke Li,[†,‡] Jiachen Huang,[†,‡] Huawei Hu,[†] Guangye Zhang,[†] Tingxuan Ma,[†] Philip C. Y. Chow,[†] Harald Ade,[#] Ding Pan,[§,†] and He Yan*[,†]

[†]Department of Chemistry and Hong Kong Branch of Chinese National Engineering Research Center for Tissue Restoration & Reconstruction, Hong Kong University of Science and Technology, Clear Water Bay, Kowloon, Hong Kong

[§]Department of Physics, Hong Kong University of Science and Technology, Clear Water Bay, Kowloon, Hong Kong

[#]Department of Physics, North Carolina State University, Raleigh, North Carolina 27695, United States

Supporting Information

ABSTRACT: We report a novel small molecule acceptor (SMA) named FTTB-PDI4 obtained via ring-fusion between the thiophene and perylene diimide (PDI) units of a PDI-tetramer with a tetrathienylbezene (TTB) core. A small voltage loss of 0.53 V and a high power conversion efficiency of 10.58% were achieved, which is the highest value reported for PDI-based devices to date. By comparing the fused and nonfused SMAs, we show that the ring-fusion introduces several beneficial effects on the properties and performances of the acceptor material, including more favorable energy levels, enhanced light absorption and stronger intermolecular packing. Interestingly, morphology data reveal that the fused molecule yields higher domain purity and thus can better maintain its molecular packing and electron mobility in the blend. Theoretical calculations also demonstrate that FTTB-PDI4 exhibits a "double-decker" geometry with two pairs of mostly parallel PDI units, which is distinctively different from reported PDI-tetramers with highly twisted geometries and can explain the better performance of the material. This work highlights the promising design of PDI-based acceptors by the ring-fusion strategy.

Conventional organic solar cells (OSCs) based on fullerene derivatives have achieved great successes with their power conversion efficiencies (PCEs) reaching beyond 10% in the past decade.[1−4] However, fullerene acceptors have several drawbacks, including low absorbance in the visible region, costly production and purification processes, relatively large voltage losses (V_{loss}) and morphological instability.[5,6] These issues limit the performances and practical applications of fullerene-based OSCs, and further development of OSCs requires an alternative strategy. Recently, nonfullerene small molecule acceptors (SMAs) have emerged as promising alternatives to fullerene derivatives, and nonfullerene OSCs can now achieve higher PCEs (>12%) than fullerene-based ones.[7−10] These exciting accomplishments can be attributed to the development of high-performance SMAs with tunable absorption, energy levels and morphological properties that can match well with donor polymers.

Perylene diimide (PDI) is one of the most investigated electron-accepting units for constructing *n*-type semiconductors.[11−15] Early generations of PDI-based SMAs exhibit large coplanar molecular structures and high crystallinity, which results in excessively strong aggregation and thus micrometer-sized phase separation between the donor and acceptor materials.[16] This is undesirable for OSC operation, given that the exciton diffusion length in organic semiconductors are typically within ∼20 nm. To address this problem, the OSC community has been developing various strategies to reduce the intermolecular interactions and excessive domain sizes of PDI-based SMAs.[17−20] One example is the design of PDI-tetramers by connecting four PDI units with a congested core. These molecules exhibit highly twisted three-dimensional geometries that effectively reduce their intermolecular interaction, thus leading to bulk heterojunction with small domain sizes. Although the introduction of intramolecular twisting enables small domain sizes, it may have detrimental effects on intermolecular $\pi-\pi$ stacking and thus charge transport ability of the acceptors in the blend.[21,22] This is clearly demonstrated for a series of PDI-tetramers (TPC-PDI4, TPE-PDI4, TPPz-PDI4, Figure S1), which show that decreasing intramolecular twisting leads to higher electron mobilities, fill factors (FF) and device performances.[22] These results indicate that researchers should minimize the intramolecular twisting of PDI-tetramers to maximize the charge transport ability of the SMAs, with the condition that a sufficiently small domain size can be achieved simultaneously.

In this Communication, we report the design, synthesis and device performances of two novel PDI-tetramers with fused and nonfused structures based on a tetrathienylbenzene (TTB) core. For the nonfused PDI-tetramer, TTB-PDI4, the single bonds between the thiophene and benzene, and thiophene and PDI units can freely rotate, which leads to a highly twisted molecular geometry similar to reported PDI-tetramers.[17,21,22] For the fused PDI-tetramer, FTTB-PDI4, however, the ring-fusion eliminates the rotational freedom between the thiophene and PDI units, resulting in a completely different molecular geometry. Density-functional theory (DFT) calculations show that FTTB-PDI4 exhibits a "double-decker" geometry containing two pairs of mostly parallel PDI units. The ring-fusion introduces several positive effects. First, the less twisted intramolecular geometry of FTTB-PDI4 leads to better charge transport ability and higher

Received: September 19, 2017
Published: November 7, 2017

DOI: 10.1021/jacs.7b09998
J. Am. Chem. Soc. 2017, 139, 16092−16095

electron mobilities in the blend film. In addition, the LUMO level of FTTB-PDI4 is upshifted, which improves the open-circuit voltages (V_{OC}) of the cells. Lastly, the blue-shifted and stronger absorption of FTTB-PDI4 result in higher short-circuit current density (J_{SC}). Overall, these beneficial changes upon ring-fusion lead to dramatically improved efficiencies from 7.11% to 10.58%, which is the highest value for PDI-based acceptors to date. Importantly, the V_{loss} of this nonfullerene device is only 0.53 V, which is among the smallest for efficient OSCs.

The synthetic route to TTB-PDI4 and FTTB-PDI4 is illustrated in Figure 1. The nonfused TTB-PDI4 was readily

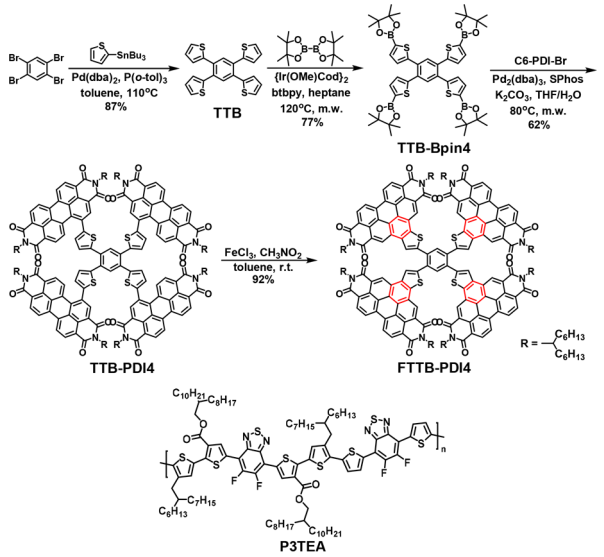

Figure 1. Synthesis of FTTB-PDI4 and the structure of P3TEA.

synthesized in 62% yield via a Suzuki reaction between TTB-Bpin4 and monobromo-PDI. Thereafter, TTB-PDI4 was treated with $FeCl_3/CH_3NO_2$ and a cyclization reaction occurred between the PDI subunits and the neighboring thiophene spacers, generating the fused structure of FTTB-PDI4 in 92% yield. Both SMAs exhibit good solubility in common organic solvents (e.g., TTB-PDI4/FTTB-PDI4:372/316 mg/mL in chloroform and 307/258 mg/mL in toluene).

The optimized geometries of TTB-PDI4 and FTTB-PDI4 from DFT calculations are illustrated in Figure 2a,b, respectively, with all alkyl chains replaced by methyl group for simplicity. TTB-PDI4 exhibits a highly twisted geometry with a high degree of rotational freedom, which is similar to the "propeller" geometries of reported PDI-tetramers.[17,21,22] After ring-fusion, the rotation between PDI and thiophene is completely locked, which leads to less intramolecular twisting for FTTB-PDI4.[18,23−26] Interestingly, the two PDI units on the same side of the benzene core are mostly parallel with partial overlapping. The overall geometry of FTTB-PDI4 resembles a "double-decker" structure, which is distinctively different from the nonfused analog and reported highly twisted PDI-tetramers.[17,21,22] Such a geometry should improve both intramolecular and intermolecular packing, which is beneficial for enhancing the charge transport ability of the SMA. In addition, the distribution of the frontier molecular orbitals of the fused and nonfused SMAs are also significantly different (Figure 2c,d). For TTB-PDI4, its HOMO and LUMO are located separately on the different parts of the molecule due to the highly

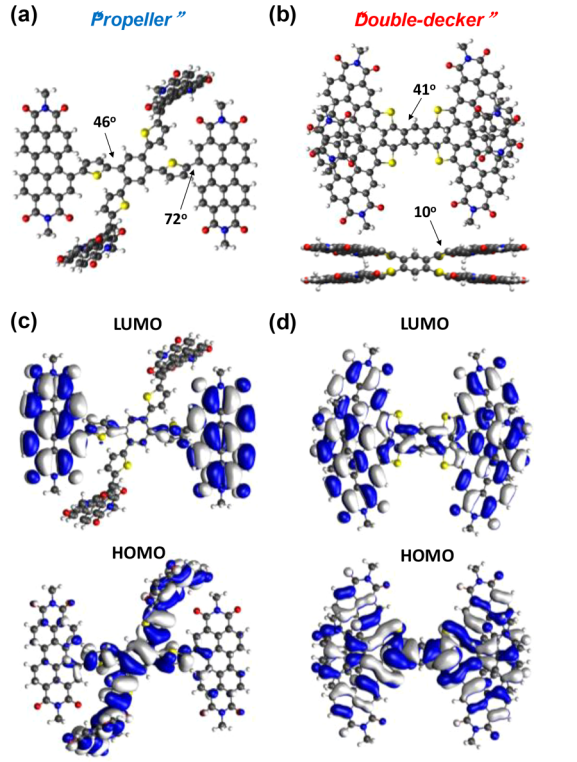

Figure 2. Optimized geometry of (a) TTB-PDI4 and (b) FTTB-PDI4. Frontier molecular orbitals of (c) TTB-PDI4 and (d) FTTB-PDI4.

twisted geometry and less effective conjugation along the molecular backbone. In contrast, the HOMO and LUMO of FTTB-PDI4 delocalize throughout the entire molecule with significant overlapping, which should enhance the absorption of FTTB-PDI4 and facilitate photon harvesting.[27] These calculation results are also supported by the experimental data on the electronic and optical properties of the two SMAs discussed below.

As shown in Figure 3a, the UV−vis absorption spectra of the TTB-PDI4 and FTTB-PDI4 pristine films exhibit dramatic differences. FTTB-PDI4 exhibits much higher absorption

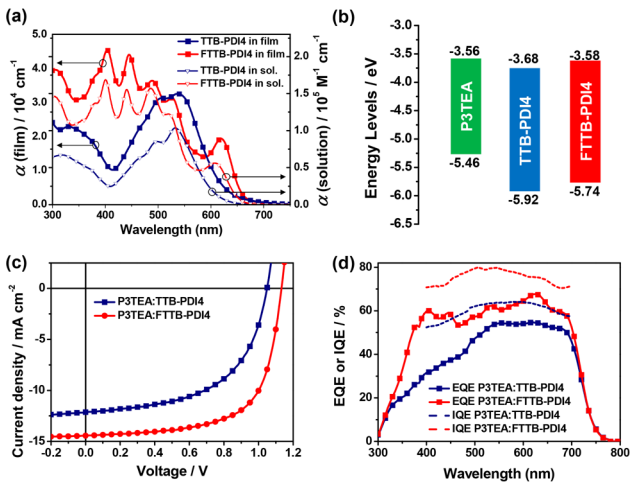

Figure 3. (a) Absorption spectra of TTB-PDI4 and FTTB-PDI4 in solution and film, (b) energy levels of P3TEA, TTB-PDI4 and FTTB-PDI4, (c) $J-V$ characteristic curves, and (d) EQE spectra of the P3TEA:TTB-PDI4 and P3TEA:FTTB-PDI4 devices.

DOI: 10.1021/jacs.7b09998
J. Am. Chem. Soc. 2017, 139, 16092−16095

Table 1. Photovoltaic Parameters of the P3TEA:TTB-PDI4, P3TEA:FTTB-PDI4 and P3TEA:$PC_{71}BM$ Devices[a]

acceptor	V_{OC} (V)	J_{SC} (mA cm^{-2})	FF (%)	PCE (%)
TTB-PDI4	1.05 ± 0.01	12.06 ± 0.13	52.9 ± 2.1	6.67 ± 0.27 (7.11)
FTTB-PDI4	1.13 ± 0.01	13.89 ± 0.16	65.9 ± 0.5	10.37 ± 0.14 (10.58)
$PC_{71}BM$	0.90 ± 0.01	12.41 ± 0.17	69.6 ± 0.1	7.73 ± 0.05(7.80)

[a]Average values obtained from 20 devices. The highest PCEs value are shown in parentheses.

coefficients compared to TTB-PDI4 (4.59 and 3.27 × 10^4 cm^{-1} in thin-film, respectively; 1.68 and 1.04 × 10^5 M^{-1} cm^{-1} in solution, respectively, Table S1). Besides, though TTB-PDI4 exhibits a broad absorption peak in 400−600 nm, FTTB-PDI4 shows multiple sharp, intense and blue-shifted peaks in 350−550 nm. Regarding the electrochemical properties, the LUMO/HOMO levels of TTB-PDI4 and FTTB-PDI4 were estimated from cyclic voltammetry (CV, Figure S2) to be −3.68/−5.92 and −3.58/−5.74 eV, respectively (Figure 3b), indicating that FTTB-PDI4 has upshifted LUMO levels relative to TTB-PDI4. The stronger absorption and upshifted LUMO level of FTTB-PDI4 can be attributed to the delocalization of frontier molecular orbitals of the PDI and the electron-donating thiophene units, leading to an enhanced V_{OC} and J_{SC} of the devices.[25,26,28−30]

The photovoltaic parameters and typical $J-V$ characteristics of the P3TEA:TTB-PDI4 and P3TEA:FTTB-PDI4 devices are shown in Table 1 and Figure 3c, respectively. All devices were optimized by using 1,8-octanedithiol as solvent additive and thermal annealing (Figures S3−S5 and Table S2). The optimized P3TEA:FTTB-PDI4 devices exhibit an averaged PCE of 10.37% with the highest PCE of 10.58%, which is higher than that of the P3TEA:TTB-PDI4 devices with an averaged PCE of 6.67%. The large enhancement of PCEs upon ring-fusion of TTB-PDI4 can be attributed to the overall improvement of V_{OC}, J_{SC} and FF in the P3TEA:FTTB-PDI4 devices. A high V_{OC} of 1.13 V was obtained for the P3TEA:FTTB-PDI4 devices, and thus the V_{loss} was calculated to be 0.53 V (by $V_{loss} = E_g/q - V_{OC}$, where E_g is the optical bandgap of P3TEA of 1.66 eV determined by the absorption onset of the film).[31] This V_{loss} value is among the lowest for efficient OSCs with low voltage losses.[31−33] Despite the low V_{loss}, the P3TEA:FTTB-PDI4 devices achieve higher J_{SC} and FF (13.89 mA cm^{-2} and 65.9%, respectively) than the P3TEA:TTB-PDI4 devices (12.06 mA cm^{-2} and 52.9%, respectively). Besides, the P3TEA:FTTB-PDI4 device exhibits higher external and internal quantum efficiencies (IQE = 80% and EQE = 68%) than the P3TEA:TTB-PDI4 devices (IQE = 64% and EQE = 55%), especially in the range of 350−500 nm due to the intense absorption of FTTB-PDI4 (Figure 3d). In addition, compared with the P3TEA:$PC_{71}BM$ devices, the P3TEA:FTTB-PDI4 devices exhibit higher V_{OC} and J_{SC} due to the better energetic and absorption match between the donor and acceptor, which demonstrates that FTTB-PDI4 is a promising alternative to fullerene.

Space-charge-limited current (SCLC) mobilities of the pristine and blend films of two SMAs are summarized in Table S3. For the pristine films, TTB-PDI4 and FTTB-PDI4 exhibit comparable electron mobilities (μ_e) of (2.1 ± 1.0) × 10^{-4} and (2.2 ± 1.5) × 10^{-4} cm^2 V^{-1} s^{-1}, respectively, suggesting their similar molecular packing in pristine films. However, when blending with P3TEA, the μ_e of the P3TEA:TTB-PDI4 blend significantly decreases by 1 order of magnitude to (3.7 ± 1.1) × 10^{-5} cm^2 V^{-1} s^{-1}, whereas the P3TEA:FTTB-PDI4 blend maintains relatively higher μ_e of (1.1 ± 0.2) × 10^{-4} cm^2 V^{-1} s^{-1}. As a result, the P3TEA:FTTB-PDI4 blend shows more balanced hole and electron mobilities (μ_h/μ_e = 1.4) than the P3TEA:TTB-PDI4 blend (μ_h/μ_e = 3.0). This indicates that FTTB-PDI4 can better maintain its molecular packing in the blend, which is supported by the morphology characterizations disscussed below.

To understand the different electron transporting properties of the two SMAs in pristine and blend films, we used resonant soft X-ray scattering (RSoXS) to investigate the domain spacing and domain purity of the blend films (Figure 4a). The domain

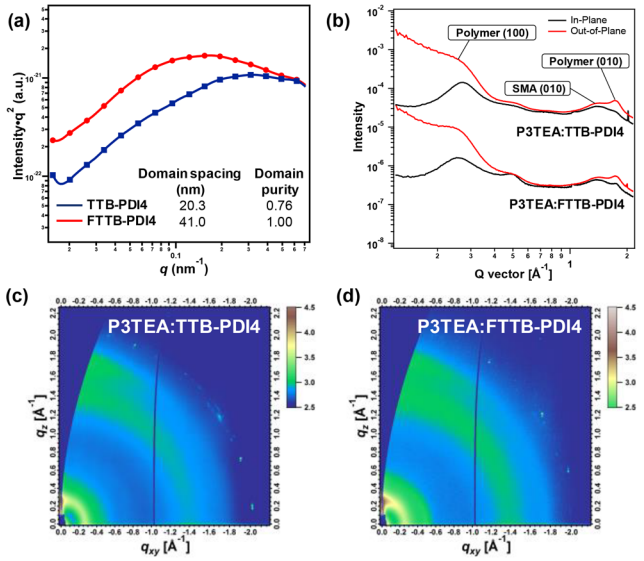

Figure 4. (a) RSoXS profiles, (b) 1D GIWAXS profiles of the in-plane and out-of-plane directions of P3TEA:TTB-PDI4 and P3TEA:FTTB-PDI4, (c) 2D GIWAXS pattern of P3TEA:TTB-PDI4 and (d) 2D GIWAXS pattern of P3TEA:FTTB-PDI4.

purity of P3TEA:FTTB-PDI4 is 24% higher than that of P3TEA:TTB-PDI4. Besides, P3TEA:FTTB-PDI4 exhibits a larger domain spacing compared to P3TEA:TTB-PDI4 (41.0 vs 20.3 nm). These data show that the fused molecule can form pure domains without excessive intermixing with the polymer, which helps maintain its molecular packing and electron mobility in the blend. Whereas, TTB-PDI4 can generate conformational isomers due to the free rotation of the PDI units, thus deteriorating the intermolecular packing and charge transport network.[23,24] In addition, the grazing incidence wide-angle X-ray scattering (GIWAXS) profiles of the two blends (Figure 4b−d) show that FTTB-PDI4 exhibits a slightly larger (010) coherence length than TTB-PDI4 (1.5 vs 1.3 nm), which also demonstrates the improved molecular packing of FTTB-PDI4 in the blends. Therefore, the intentionally reduced intramolecular twisting of FTTB-PDI4 enables the formation of pure yet reasonably small domains, thus maximizing the charge mobilities and device performances.

In conclusion, we designed and synthesized two PDI-tetramers with fused and nonfused structures. DFT calculations reveal that the fused FTTB-PDI4 displays reduced intra-

DOI: 10.1021/jacs.7b09998
J. Am. Chem. Soc. 2017, 139, 16092−16095

molecular twisting compared with TTB-PDI4, which results in stronger $\pi-\pi$ stacking and higher domain purity in the P3TEA:FTTB-PDI4 blend. In addition, FTTB-PDI4 exhibits blue-shifted absorption, high absorptivity and upshifted energy levels, which enables a complementary absorption and energetic match with P3TEA. Consequently, the P3TEA:FTTB-PDI4 devices achieve the highest PCE of 10.58% with a small voltage loss of 0.53 V but reasonably high J_{SC} of 13.89 mA cm^{-2} and FF of 65.9%. In comparison, the highest PCE of the P3TEA:TTB-PDI4 devices is only 7.11%, which is 49% lower than that of the P3TEA:FTTB-PDI4 ones. The substantial differences in photovoltaic performances between TTB-PDI4 and FTTB-PDI4 highlight the importance of modulating the intramolecular twisting and the ring-fusion strategy in the design of novel PDI-based SMAs.

■ ASSOCIATED CONTENT

Supporting Information

The Supporting Information is available free of charge on the ACS Publications website at DOI: 10.1021/jacs.7b09998.

Synthesis, absorption spectra, photoluminescence spectra, mobilities, electrochemical measurement, theoretical calculations and device fabrication (PDF)

■ AUTHOR INFORMATION

Corresponding Author

*hyan@ust.hk

ORCID

Jianquan Zhang: 0000-0003-4528-9824

Huawei Hu: 0000-0002-9790-8837

He Yan: 0000-0003-1780-8308

Author Contributions

‡J.Z., Y.L. and J.H. contributed equally to this work.

Notes

The authors declare no competing financial interest.

■ ACKNOWLEDGMENTS

The work described in this paper was partially supported by the National Basic Research Program of China (973 Program; 2013CB834701 and 2014CB643501), the Hong Kong Research Grants Council (T23−407/13 N, N_HKUST623/13, 16305915, 16322416, 606012 and 16303917), HK JEBN Limited, HKUST president's office (Project FP201) and the National Science Foundation of China (#21374090) Hong Kong Innovation and Technology Commission (ITC-CNERC14SC01 and ITS/083/15). X-ray data acquired at beamlines 11.0.1.2. and 7.3.3. at the ALS in LBNL, supported by the U.S. DOE (DE-AC02-05CH11231).

■ REFERENCES

(1) He, Z. C.; Xiao, B.; Liu, F.; Wu, H. B.; Yang, Y. L.; Xiao, S.; Wang, C.; Russell, T. P.; Cao, Y. *Nat. Photonics* **2015**, *9*, 174.

(2) Zhao, J. B.; Li, Y. K.; Yang, G. F.; Jiang, K.; Lin, H. R.; Ade, H.; Ma, W.; Yan, H. *Nat. Energy* **2016**, *1*, 15027.

(3) Hu, H.; Jiang, K.; Yang, G.; Liu, J.; Li, Z.; Lin, H.; Liu, Y.; Zhao, J.; Zhang, J.; Huang, F.; Qu, Y.; Ma, W.; Yan, H. *J. Am. Chem. Soc.* **2015**, *137*, 14149.

(4) Liu, Y.; Zhao, J.; Li, Z.; Mu, C.; Ma, W.; Hu, H.; Jiang, K.; Lin, H.; Ade, H.; Yan, H. *Nat. Commun.* **2014**, *5*, 5293.

(5) Sauve, G.; Fernando, R. *J. Phys. Chem. Lett.* **2015**, *6*, 3770.

(6) Nielsen, C. B.; Holliday, S.; Chen, H. Y.; Cryer, S. J.; McCulloch, I. *Acc. Chem. Res.* **2015**, *48*, 2803.

(7) Li, S.; Ye, L.; Zhao, W.; Zhang, S.; Mukherjee, S.; Ade, H.; Hou, J. *Adv. Mater.* **2016**, *28*, 9423.

(8) Yang, Y.; Zhang, Z. G.; Bin, H.; Chen, S.; Gao, L.; Xue, L.; Yang, C.; Li, Y. *J. Am. Chem. Soc.* **2016**, *138*, 15011.

(9) Zhao, F. W.; Dai, S. X.; Wu, Y. Q.; Zhang, Q. Q.; Wang, J. Y.; Jiang, L.; Ling, Q. D.; Wei, Z. X.; Ma, W.; You, W.; Wang, C. R.; Zhan, X. W. *Adv. Mater.* **2017**, *29*, 1700144.

(10) Zhao, W.; Li, S.; Yao, H.; Zhang, S.; Zhang, Y.; Yang, B.; Hou, J. *J. Am. Chem. Soc.* **2017**, *139*, 7148.

(11) Li, C.; Wonneberger, H. *Adv. Mater.* **2012**, *24*, 613.

(12) Zhan, X.; Facchetti, A.; Barlow, S.; Marks, T. J.; Ratner, M. A.; Wasielewski, M. R.; Marder, S. R. *Adv. Mater.* **2011**, *23*, 268.

(13) Anthony, J. E.; Facchetti, A.; Heeney, M.; Marder, S. R.; Zhan, X. *Adv. Mater.* **2010**, *22*, 3876.

(14) Weil, T.; Vosch, T.; Hofkens, J.; Peneva, K.; Müllen, K. *Angew. Chem., Int. Ed.* **2010**, *49*, 9068.

(15) Huang, C.; Barlow, S.; Marder, S. R. *J. Org. Chem.* **2011**, *76*, 2386.

(16) Rajaram, S.; Shivanna, R.; Kandappa, S. K.; Narayan, K. S. *J. Phys. Chem. Lett.* **2012**, *3*, 2405.

(17) Liu, Y.; Mu, C.; Jiang, K.; Zhao, J.; Li, Y.; Zhang, L.; Li, Z.; Lai, J. Y.; Hu, H.; Ma, T.; Hu, R.; Yu, D.; Huang, X.; Tang, B. Z.; Yan, H. *Adv. Mater.* **2015**, *27*, 1015.

(18) Zhong, Y.; Trinh, M. T.; Chen, R.; Wang, W.; Khlyabich, P. P.; Kumar, B.; Xu, Q.; Nam, C. Y.; Sfeir, M. Y.; Black, C.; Steigerwald, M. L.; Loo, Y. L.; Xiao, S.; Ng, F.; Zhu, X. Y.; Nuckolls, C. *J. Am. Chem. Soc.* **2014**, *136*, 15215.

(19) Meng, D.; Sun, D.; Zhong, C.; Liu, T.; Fan, B.; Huo, L.; Li, Y.; Jiang, W.; Choi, H.; Kim, T.; Kim, J. Y.; Sun, Y.; Wang, Z.; Heeger, A. J. *J. Am. Chem. Soc.* **2016**, *138*, 375.

(20) Sun, D.; Meng, D.; Cai, Y.; Fan, B.; Li, Y.; Jiang, W.; Huo, L.; Sun, Y.; Wang, Z. *J. Am. Chem. Soc.* **2015**, *137*, 11156.

(21) Wu, Q.; Zhao, D.; Schneider, A. M.; Chen, W.; Yu, L. *J. Am. Chem. Soc.* **2016**, *138*, 7248.

(22) Lin, H.; Chen, S.; Hu, H.; Zhang, L.; Ma, T.; Lai, J. Y.; Li, Z.; Qin, A.; Huang, X.; Tang, B.; Yan, H. *Adv. Mater.* **2016**, *28*, 8546.

(23) Zhong, H.; Wu, C. H.; Li, C. Z.; Carpenter, J.; Chueh, C. C.; Chen, J. Y.; Ade, H.; Jen, A. K. *Adv. Mater.* **2016**, *28*, 951.

(24) Wu, Q. H.; Zhao, D. L.; Yang, J. H.; Sharapov, V.; Cai, Z.; Li, L. W.; Zhang, N.; Neshchadin, A.; Chen, W.; Yu, L. P. *Chem. Mater.* **2017**, *29*, 1127.

(25) Meng, D.; Fu, H.; Xiao, C.; Meng, X.; Winands, T.; Ma, W.; Wei, W.; Fan, B.; Huo, L.; Doltsinis, N. L.; Li, Y.; Sun, Y.; Wang, Z. *J. Am. Chem. Soc.* **2016**, *138*, 10184.

(26) Hartnett, P. E.; Matte, H. S. S. R.; Eastham, N. D.; Jackson, N. E.; Wu, Y. L.; Chen, L. X.; Ratner, M. A.; Chang, R. P. H.; Hersam, M. C.; Wasielewski, M. R.; Marks, T. J. *Chem. Sci.* **2016**, *7*, 3543.

(27) Pandey, L.; Risko, C.; Norton, J. E.; Brédas, J.-L. *Macromolecules* **2012**, *45*, 6405.

(28) Zhong, Y.; Kumar, B.; Oh, S.; Trinh, M. T.; Wu, Y.; Elbert, K.; Li, P.; Zhu, X.; Xiao, S.; Ng, F.; Steigerwald, M. L.; Nuckolls, C. *J. Am. Chem. Soc.* **2014**, *136*, 8122.

(29) Nolde, F.; Pisula, W.; Muller, S.; Kohl, C.; Mullen, K. *Chem. Mater.* **2006**, *18*, 3715.

(30) Sisto, T. J.; Zhong, Y.; Zhang, B.; Trinh, M. T.; Miyata, K.; Zhong, X.; Zhu, X. Y.; Steigerwald, M. L.; Ng, F.; Nuckolls, C. *J. Am. Chem. Soc.* **2017**, *139*, 5648.

(31) Liu, J.; Chen, S. S.; Qian, D. P.; Gautam, B.; Yang, G. F.; Zhao, J. B.; Bergqvist, J.; Zhang, F. L.; Ma, W.; Ade, H.; Inganas, O.; Gundogdu, K.; Gao, F.; Yan, H. *Nat. Energy* **2016**, *1*, 16089.

(32) Chen, S.; Liu, Y.; Zhang, L.; Chow, P. C. Y.; Wang, Z.; Zhang, G.; Ma, W.; Yan, H. *J. Am. Chem. Soc.* **2017**, *139*, 6298.

(33) Baran, D.; Kirchartz, T.; Wheeler, S.; Dimitrov, S.; Abdelsamie, M.; Gorman, J.; Ashraf, R. S.; Holliday, S.; Wadsworth, A.; Gasparini, N.; Kaienburg, P.; Yan, H.; Amassian, A.; Brabec, C. J.; Durrant, J. R.; McCulloch, I. *Energy Environ. Sci.* **2016**, *9*, 3783.

DOI: 10.1021/jacs.7b09998
J. Am. Chem. Soc. 2017, 139, 16092−16095